MCLAFFERTY REARRANGEMENT OF PEPTIDES AND SUBSTITUENT EFFECTS ON PEPTIDE FRAGMENTATION: THEORETICAL AND EXPERIMENTAL INVESTIGATIONS

A Thesis by

Dale Kerstetter

Bachelor of General Studies, Wichita State University, 2007

Submitted to the Department of Chemistry
and the faculty of the Graduate School of
Wichita State University
in partial fulfillment
of the requirements for the degree of
Master of Science

December 2009

© Copyright 2009 by Dale Kerstetter

All Rights Reserved

MCLAFFERTY REARRANGEMENT AND SUBSTITUENT EFFECTS ON PEPTIDE FRAGMENTATION: THEORETICAL AND EXPERIMENTAL INVESTIGATIONS

The following faculty members have examined the final copy of this thesis for form and content, and recommend that it be accepted in partial fulfillment of the requirement for the degree of Master of Science, with a major in Chemistry.

_____

Michael Van Stipdonk, Committee Chair

_____

David Eichhorn, Committee Member

_____

Francis D'Souza, Committee Member

_____

Erach Talaty, Committee Member

_____

Jeffrey May, Committee Member

ACKNOWLEDGEMENTS

I would like to thank my research advisor Dr. Michael van Stipdonk for his guidance and support. I thank all the members of the Van Stipdonk research group over the past couple years for their support and help, especially Justin Lygrisse, Ryan Dain, Sarah Young, and Kelsey Witherspoon. I would also like to thank the office staff and stock room staff for the support they provide to the department. I would like to thank my thesis committee members Dr. Eichhorn, Dr. Talaty, Dr. May, and Dr. D'Souza for their support. I would like to thank all of the faculty and graduate students at the WSU chemistry department for their support and making this program possible.

I would like to thank my family for their support. I would especially like to thank my wife, Sarah, for her continual support and encouragement throughout my studies.

ABSTRACT

The research presented here details two studies that utilized theoretical analysis and experimentation to further the understanding of peptide fragmentation. The first study was the McLafferty rearrangement, which involves transfer of a γ-position hydrogen atom to a carbonyl oxygen atom through a cyclic intermediate, followed by the elimination of an alkene. The second study examined substituent effects on benzene ring terminated peptides.

TABLE OF CONTENTS

Chapter			Page
1	INTRODUCTION		
	1.1	General Introduction	1
	1.2	Mass Spectrometry	2
	1.3	Computational Chemistry and Molecular Modeling	4
	1.4	McLafferty Rearrangement	4
	1.5	Substituent Effects	5
	1.6	Peptide Nomenclature	7
2	EXPERIMENTAL		
	2.1	Materials and Methods-McLafferty Rearrangement	8
		2.1.1 Peptide Synthesis	8
		2.1.2 Mass Spectrometry	8
		2.1.3 Infrared Multi-photon Photodissociation (IRMPD) experiment	9
		2.1.4 Molecular structure and Frequency Calculations (Computational)	11
	2.2	Materials and Methods-Substituent Effects	13
		2.2.1 Peptide Synthesis/Mass Spectrometry	13
		2.2.2 Kinetics	13
		2.2.3 Molecular Modeling	14
3	RESULTS		
	3.1	McLafferty	15
	3.2	Substituent Effects	27
4	Summary		
	4.1	McLafferty	34
	4.2	Substituent Effects	34
Bibliography			35

LIST OF FIGURES

Figure		Page
1.1	General representation of the McLafferty rearrangement.	5
1.2	Structure of NicGO*t*Bu.	5
1.3	Structure of BetGO*t*Bu$^+$.	5
1.4	Peptide nomenclature illustration [11-13].	7
3.1	Tandem mass spectra starting from the protonated nicotinyl-glycine-*tert*-butyl ester (NicGOtBu+H)$^+$ using the quadrupole ion trap mass spectrometer: (a) dissociation of (NicGO*t*Bu+H)$^+$; (b) dissociation (MS^3 stage) of (NicGOH+H)$^+$, product resulting from McLafferty rearrangement.	16
3.2	Tandem mass spectra starting from the betaine-glycine-*tert*-butyl ester (BetGOtBu+H)$^+$ using the quadrupole ion trap mass spectrometer: (a) dissociation of (BetGO*t*Bu+H)$^+$; (b) dissociation (MS^3 stage) of (BetGOH+H)$^+$, product resulting from McLafferty rearrangement.	17
3.3	Tandem mass spectra starting from fully deuterium-exchanged nicotinyl-glycine-*tert*-butyl ester d2-(NicGOtBu+H)+ using the quadrupole ion trap mass spectrometer: (a) dissociation of d2-(NicGOtBu+H)+ , (b) dissociation (MS3 stage) of (NicGOH+H)+ product resulting from McLafferty rearrangement.	19
3.4	Tandem mass spectra starting from fully deuterium-exchanged betaine-glycine-*tert*-butyl ester d2-(BetGOtBu+H)+ using the quadrupole ion trap mass spectrometer: (a) dissociation of d2-(BetGOtBu+H)+ , (b) dissociation (MS3 stage) of (BetGOH+H)+ product resulting from McLafferty rearrangement.	20
3.5	Potential conformations (Nic_a, Nic_b, Nic_c, Nic_d, Nic_d, Nic_e, Nic_f, Nic_g, Nic_h, and Nic_i) for (NicGOH+H)$^+$ as determined using DFT (B3LYP/6-311+g(d,p)).	21
3.6	Comparison between IRMPD spectrum generated from (NicGOH+H)$^+$ (a) and theoretical spectra based on DFT calculations for structures: (b) Nic_a, (c) Nic_b, (d) Nic_c and (e) Nic_d.	22

LIST OF FIGURES (Continued)

Figure		Page
3.7	Comparison between IRMPD spectrum generated from BetGOH (a) and theoretical spectra based on DFT calculations for structures: (b) Bet_a and (c) Bet_b.	23
3.8	Potential conformations for $(BetGOH)^+$ as determined using DFT (B3LYP/6-311+g(d,p)).	23
3.9	Comparison between IRMPD spectrum generated from d_2-$(NicGOH+H)^+$ (a) and theoretical spectra based on DFT calculations for 3 different labeled isomers: (b) ring D, amide D and acid H; (c) ring D, amide H and acid D and (d) ring H, amide D and acid D.	23
3.10	Comparison between IRMPD spectrum generated from d_1-$(BetGOH)^+$ (a) and theoretical spectra based on DFT calculations for 3 different labeled isomers: (b) amide D and acid H and (c) amide H and acid D.	23
3.11	Comparison between IRMPD spectrum generated from $(NicGOH+H)^+$ (a) and theoretical spectra based on DFT calculations for structures: (b) Nic_e, (c) Nic_f, (d) Nic_g, (e) Nic_h, and (f) Nic_i. Conformations of Nic_a, Nic_b, Nic_c and Nic_d are provided in Figure 2.2.	24
3.12	MS/MS comparison pTolGOMe to 3FpTolGOMe.	28
3.13	MS/MS comparison mTolGOMe to 3FmTolGOMe.	28
3.14	Double resonance experiment of pTolGOMe.	29
3.15	Pseudo DFT Ea vs. Berkley Madonna pseudo Ea.	33
3.16	Relative b^+ ion abundance as a function of volts.	33

LIST OF SCHEMES

Scheme		Page
3.1	Dissociation pathway for (NicGO*t*Bu+H)$^+$ showing McLafferty rearrangement and formation of b_2^+ and a_2^+ via the "oxazolone" pathway.	17
3.2	Pathway for formation of b^+ ion (3F*m*TolGOMe).	30

LIST OF TABLES

Table		Page
3.1	Relative Energies of $(NicGOH+H)^+$ conformational isomers.	21
3.2	Relative energies of $(BetGOH)^+$ conformational isomers.	24
3.3	b^+ ion Relative energies with ZPE.	31
3.4	Berkley Madonna pseudo rate constants for the formation of the b^+ ion.	32
3.5	Berkley Madonna pseudo Ea for the formation of the b^+ ion.	32

LIST OF EQUATIONS

Equation		Page
3.1	Curve fit error	30

LIST OF ABBREVIATIONS

1	DI	Deionized
2	µL	Microliter
3	µM	Micromolar
4	° C	Celsius
5	*tert*	tertiary
6	CID	Collision induced dissociation
7	cm	Centimeter
8	D	Deuterium
9	D_2O	Deuterium oxide
10	H	Hydrogen
11	MS	Mass spectrometry
12	ESI	Electrospray ionization
13	g	Gram
14	V	Volts
15	kV	Kilovolts
16	L	Liter
17	M	Molar
18	m/z	Mass to charge ratio
19	mg	Milligram
20	min	Minute
21	mL	Milliliter

22	mm	Millimeter
23	mM	Millimolar
24	ms	Millisecond
25	N_2	Nitrogen gas
26	HDX	hydrogen for deuterium exchange

CHAPTER 1

INTRODUCTION

1.1 General Introduction

Proteins represent a diverse group of structural and functional molecules that are essential to living organisms. The proteome of an organism is a record of those proteins coded for and otherwise expressed by a given genome. Proteomics, then is the study of a proteome, whether to gain detailed information of the proteins produced by the genome, or of the a group or groups of proteins are involved in various physical states of an organism. At the heart of proteomics is the rapid and accurate identification of proteins, and the more widely applied analytical tool for characterization of proteins is tandem mass spectrometry, often teamed with a method of ion activation such as collision-induced dissociation (CID) or electron capture dissociation.

Regardless of the ion activation method utilized, use of tandem MS to characterize peptides requires (unimolecular) reactions to be induced within the instrument to force the fragmentation of the large biopolymers. Identification of sequence is often made either by comparing fragment ion distributions from an unknown sample to ones that exist for known peptides in sequence data bases, or by direct interpretation of the differences in mass between fragment ions themselves, or between fragment ions and their precursors. Therefore, understanding fundamental peptide fragmentation chemistry is essential to the effective application of mass spectrometry to peptide identification [1,2]. Specific experiments designed to probe fundamental dissociation reactions of peptides using small, model systems are the focus of this thesis research. Mass spectrometry and tandem mass spectrometry were used to

study the fragmentation of model peptides. The fragmentation reactions were probed in addition using density functional theory calculations. The overall aim was to develop model systems that allow experiment and theory to be converged in the context of understanding peptide dissociation, and in particular, fragmentation mechanisms.

1.2 Mass Spectrometry

Mass spectrometry enables, in part, researchers to study large molecules such as peptides or proteins in the gas phase, outside of the influence of solvent. In order for a given peptide or protein to be analyzed it must first be volatized, then ionized to furnish a positively or negatively charged species. Rapid heating, sputtering, desorption, and electrospray are commonly used methods to volatilize molecules in condensed phases. There are numerous methods used for ionization; electron impact, chemical ionization, laser desorption, and electrospray ionization (ESI) to name a few [3,4]. ESI is one of the most commonly used ionization methods for peptides and proteins, and was utilized exclusively for the experiments described in chapters 2 and 3.

ESI-MS is achieved by applying a strong electric field under atmospheric pressure to a liquid passing through a capillary tube [3]. The liquid contains the sample or analyte in a solvent suspension. The electric field is obtained by applying a potential difference between the capillary and a counter electrode [3]. The field forces a charge accumulation on the liquid surface at the end of the capillary which then breaks into highly charged droplets [3,5]. These droplets pass through a heated capillary or a heated inert gas removing the remaining solvent [3,5]. The remaining individual charged molecules (ions) pass into a region of high-vacuum

where they are subsequently analyzed based on mass to charge (m/z) ratio and detected. A mass spectrum is produced which reports relative ion abundance versus m/z. Within the context of use of tandem MS in proteomics, the ionized analyte is then referred to as the parent ion.

As mentioned, above the analyte is in a solvent which also aids in charging the molecule. A common method to charge a molecule is to alter pH to assist protonation or deprotonation of molecules while in solution. Addition of a proton produces a gas phase species designated the protonated molecule or (M+H). Other methods to charge a molecule are by adding metals in solution, thereby adding the charge of the metal to the overall molecule, i.e. Na^+ or Ag^+. This approach is especially useful for molecules that are not very basic in the Bronsted-Lowry sense.

Tandem mass spectrometry (MS/MS) is a method utilized that involves at least two stages of mass analysis primarily in conjuction with dissociation of the parent ion [3]. It should be noted that not all mass spectrometers are capable of MS/MS and some mass spectrometers are capable of multiple tandem MS stages denoted by MS^n. The basic principle behind MS/MS is the mass analyzer isolates the parent ion which then undergoes dissociation to produce a fragment ion and a neutral fragment [3]. In MS^n instruments, the process of isolating and dissociating can be repeated numerous times depending on the instrument. One method of dissociation is collision induced dissociation (CID) where the isolated ions are put into a collisional cell where an inert gas collides with the molecule thereby increasing the molecule's internal energy leading to the fragmentation of the molecule [3]. For each tandem MS a mass analyzer sends the relative ion abundances and m/z data to the detector as mentioned above.

1.3 Computational Chemistry and Molecular Modeling

Computational chemistry can be divided into two areas: molecular modeling and molecular simulation [6]. Molecular modeling is the structural modeling part, whereas molecular simulation is the modeling of processes [6]. Areas of molecular modeling utilize various functionals and basis sets to obtain theoretical molecular information. One currently popular approach is to apply density functional theory (DFT) to predict structures (minima and transition states), relative energies, and theoretical infrared spectra. Since "electrons are quantum mechanical spin particles" [6], DFT utilizes the electron density to compute all properties of interested systems as a function of arbitrary spatial coordinates [6,7]. This is due to the fact that electrons are quantum mechanical spin particles [6]. Basis sets are generally algorithms which describe atomic orbitals [7]. Larger basis sets describe the larger atomic orbitals (d- and f-orbitals) more accurately, whereas the smaller basis sets describe the simpler orbitals sufficiently. It should be noted that the larger basis sets are less efficient with respect to the amount of time required to run the calculations.

1.4 McLafferty Rearrangement

One of the reactions investigated in this thesis is the McLafferty rearrangement, first experimentally observed by F. W. McLafferty and published in a 1956 Analytical Chemistry article [8]. The rearrangement is observed in mass spectrometry in the gas phase on a charged molecule and typically involves a three carbon (or larger) ester with the γ-hydrogen migrating to the adjacent carbonyl, thereby cleaving the ester bond and making a charged carboxylic acid and neutral alkene. The overall charge on the molecule does not change nor does the position

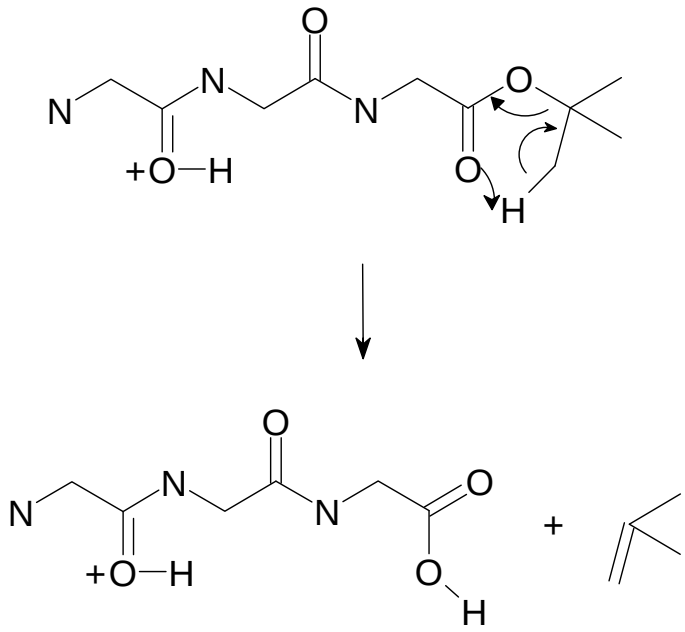

Figure 1.1-General representation of the McLafferty rearrangement.

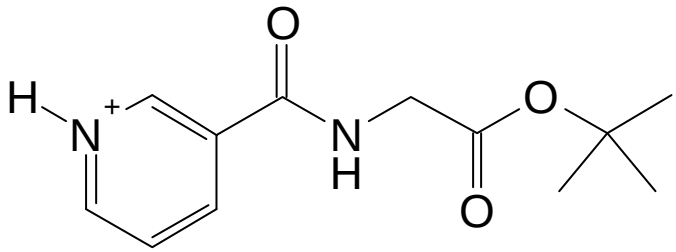

Figure 1.2-Structure of NicGO*t*Bu.

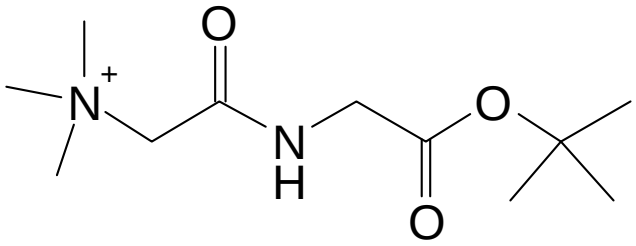

Figure 1.3-Structure of BetGO*t*Bu$^+$.

of the charge change. Figure 1.1 illustrates the general mechanism for the McLafferty rearrangement.

The model peptides studied were nicotinylglycine *tert*-butyl ester (NicGO*t*Bu, Figure 1.2) and betaineglycine *tert*-butyl ester (BetGO*t*Bu$^+$, Figure 1.3) each having nine potential γ-hydrogens to participate in the McLafferty rearrangement. The goal in this study was to use photodissociation to produce an infrared spectrum to probe H atom transfer, as well as to probe the degree of scrambling that may be occurring, and to further confirm the McLafferty rearrangement.

1.5 Substituent Effects on Fragmentation of Model Peptides

Replacing hydrogen atoms with an electron donating or electron withdrawing group induces a substituent effect on a molecule. The type of effect that takes place depends on the

group and the intensity of its electron donating or electron withdrawing capacity. If the group is on a benzene ring the position (*para*-, *meta*-, or *ortho*-) of the group also has an effect on a molecule. Particularly of interest was the role the substituent had on the nucleophillic attack to form the b^+ ion.

As part of an ongoing effort to study and understand the factors that affect fragmentation, an investigation of collision induced dissociation (CID) of variants of hippuric acid methyl ester (benzoic acid-glycine methyl ester) was undertaken. The specific goal was to determine whether the presence, identity and position of electron donating or withdrawing substituents influence the tendency for the peptides to fragment via two competing pathways by altering the strength of a specific nucleophile important to the "oxazolone" dissociation pathway to b-type ions. Previous work by Leioe *et al* has noted that there are different favoring pathways when studying substituent effects on the single amino acid, phenylalanine [9]. This is the first known study to investigate substituent effects on gas phase peptide fragmentation.

In order to study substituent effects thoroughly, the need to identify possible competing ions arose. Double resonance (DR) experimentation enables researchers to evaluate potential competing pathways for each molecule studied. In the DR experiment, excitation of a parent ion and a potential product ion is performed simultaneously [10]. Ejection of a particular product ion allows for determination of "parentage" of other products, particularly those that might be formed by a cascade of sequential fragmentation reactions.

1.6 Peptide Nomenclature

Since peptides were first analyzed in mass spectrometry, identifying the fragments became a problem due to inconsistencies in reporting the results. The most widely accepted and used peptide nomenclature is illustrated in figure 1.4 [11-13]. The location of bond cleavage or fragmentation determines the type of ion; a, b, and c ions refer to charged N-terminus fragments and the neutral loss of C-terminal residues, whereas x, y, and z ions refer to the charged C-terminus fragments and the neutral loss of N-terminal residues. Keep in mind that mass spectrometers detect ions so the observed results are the charged a, b, or c ions.

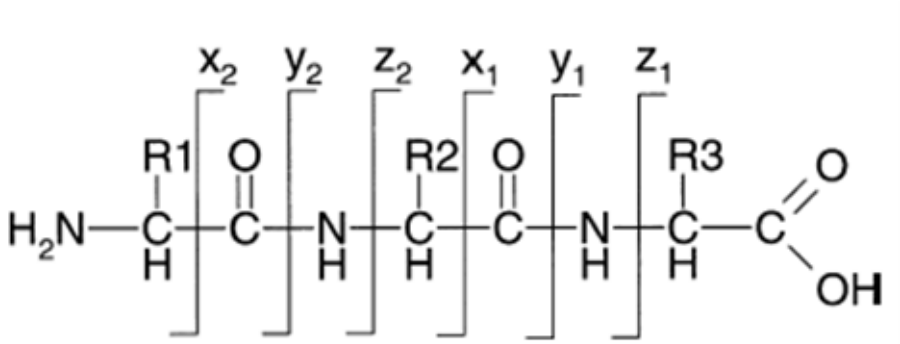

Figure 1.4-Peptide nomenclature illustration [11-13].

CHAPTER 2

EXPERIMENTAL

2.1 Materials and Methods-McLafferty Rearrangement

2.1.1 Peptide Synthesis

The peptides utilized in this study, NicGO*t*Bu and BetGO*t*Bu$^+$, were synthesized utilizing a single reaction vessel with a commercially available resin bound carbodiimide (PS-carbodiimide). The resin, acids (nicotinic acid and betaine), and amine (glycine *tert*-butyl ester) were weighed out according to a 2:1.5:1 respective ratio which was provided by the resin manufacturer, since the manufacturer did not specify what ratio to use a mass ratio was used. Each component was added to a reaction vessel along with 10 mL of dichloromethane to form a suspension and the solution was stirred for a minimum of eight hours. The solution was then filtered by vacuum filtration to remove the resin. The remaining solution was allowed to evaporate to dryness either with argon gas or left open to the air in a fume hood, leaving behind the desired peptide.

2.1.2 Mass Spectrometry

Synthesis and composition was confirmed via ESI-MS and CID of the precursor ion, M+H. ESI-MS and quadrupole ion trap CID was investigated using a Finnigan LCQ Deca ion trap mass spectrometer (ThermoFinnigan, San Jose, CA, USA). The peptides were prepared by dissolving a small amount of solid into a solution of 1:1 (V:V) methanol (CH_3OH) and DI water (H_2O) or deuterated methanol (CH_3OD) and deuterium oxide (D_2O) to obtain a final concentration in the mM region. The solutions were then infused into the ESI source using the incorporated syringe pump at a flow rate of 5 μL/min. The atmospheric pressure ionization stack settings for the

LCQ (lens voltages, quadrupole and octapole voltage offsets, etc.) were optimized for highest $(M)^+$, $(M+H)^+$, or $(M+D)^+$ ion intensity using the auto-tune routine within the LCQ Tune program. The spray needle voltage was maintained at +5 kV, N_2 sheath gas flow rate at approximately .375 L/min and the capillary (desolvation) temperature at 200° C.

For CID studies, the precursor isolation widths used were 0.8-1.0 mass to charge (m/z) units to ensure the isolation and dissociation of single isotopic peak. The normalized collision energies (which define the amplitude of R. F. voltage applied to the end cap electrodes to induced collisional activation) were set to 25 - 30% of 5 volts, which corresponds to approximately 0.65 to 0.72 V using the current instrument calibration. The activation Q setting (used to adjust the *q* parameter for the precursor ion during the CID experiment) was 0.30 and activation times of 30 msec were used.

To determine the extent to which ions undergo deuterium for hydrogen back exchange while in the ion trap, product ions generated by CID were isolated and stored, without imposed collisional activation, for periods ranging from 10 msec to 1 sec. During the isolation time, ions may react with H_2O present as a contaminant in the vacuum system. This has the potential of displaying incorrect results by adding water to the molecule and subsequently losing water the molecule can be protonated on a different location.

2.1.3 Infrared Multi-photon Photodissociation (IRMPD) experiment

A custom Fourier transform ion cyclotron resonance (FT-ICR) mass spectrometer at the FOM Institute for Plasma Physics in Nieuwegein, The Netherlands, was used for the infrared multi-photon photodissociation (IRMPD) experiments. The mass spectrometer was equipped with a commercial Z-spray electrospray ionization source (Micromass,

Manchester, U.K.) that produces ions at atmospheric pressure in a spray plume orthogonal to a sampling cone. Specific ESI operating parameters such as spray voltage, cone voltage and ion transfer lens voltages and block and nitrogen gas temperatures were adjusted empirically to maximize formation and transfer of $(M+H)^+$and $(M+D)^+$ ions to the ion cyclotron resonance cell. Peptide solutions were created as described above for the ion trap mass spectrometry studies.

The McLafferty rearrangement of the native or deuterium-exchanged peptides was effected by raising the cone voltage to induce source fragmentation. The resulting free-acid forms of the peptides were accumulated in an external hexapole for approximately 500 ms prior to being injected into the ICR cell via a 1 m octapole ion guide. Rapid switching of the DC bias of the octopole during the ion transfer allows for capture of the ions in the ICR cell without the use of a gas pulse, thus avoiding collisional heating of the ions [14]. Product ions resulting from McLafferty rearrangement induced in the ESI source region were detected in the mass spectrum, and were isolated for IRMPD study using a stored waveform inverse Fourier transform (SWIFT) pulse [15] which ejected all species except those having the desired mass.

Infrared spectra were collected by monitoring the efficiency of IRMPD as a function of laser wavelength. After mass-selective isolation, the precursor ions are irradiated using ten FELIX macropulses (40 mJ per macropulse, 5 μs pulse duration, bandwidth 0.2 – 0.5 % of central λ). IRMPD occurs through non-coherent absorption of tens to hundreds of IR photons, when the laser frequency matches a vibrational mode of the gas-phase ion. The energy is distributed over all vibrational modes by intramolecular vibrational redistribution

(IVR). The IVR process allows the energy of each photon to be "relaxed" prior to the absorption of the next photon, and thus allows promotion of the ion's internal energy to the dissociation threshold [16]. Prior studies have shown that the infrared spectra obtained using IRMPD are comparable to those obtained using linear absorption techniques [17].

To produce infrared spectra, the free electron laser was scanned in 0.02 to 0.04 μm increments between 5.5 and 8.5 μm, with measurement of product ions and un-dissociated precursor ions using the excite/detect sequence of the FT-ICR-MS [18] after irradiation with FELIX. The IRMPD yield is normalized to the total ion yield, and corrected for variations in FELIX power over the spectral range.

2.1.4 Molecular structure and Frequency Calculations (Computational)

All geometry optimizations were performed using the hybrid B3LYP functional [19,20]. Optimization of a wide range of conformational isomers of the McLafferty rearrangement products, $(NicGOH+H)^+$ and $(BetGOH)^+$, were initiated using the relatively small 3-21g* basis set. Minimized geometries from calculations at the B3LYP/3-21g* level of theory were then re-optimized using the 6-311+g(d,p) basis set. Frequency calculations were carried out at the B3LYP/6-311+g(d,p) level of theory. Vibrational spectra for the isotope-labeled peptides were calculated using the freq=read isotopes command with appropriate positioning of D atoms within optimized structures. For comparison to the experimentally derived spectra, the frequencies generated by DFT were scaled by a factor of 0.98 for inclusion into figures 3.6, 3.7, 3.9, and 3.10. As discussed below, the B3LYP functional, and the basis sets and scaling factor employed, provided good general agreement with the experimental IRMPD spectra. Because the goal here was to use the calculations to assign probable ion structures and assist with

interpretation of the IRMPD spectrum, rather than assess the absolute accuracy of theoretical methods, alternative functionals and models were not used, nor was calculation of dissociation and reaction transition state energies carried out. Coordinates for the optimized structures for each species are included in table 1 of the supporting information. All DFT calculations were performed using the Gaussian 03 group of programs [21].

2.2 Materials and Methods-Substituent Effects

2.2.1 Peptide Synthesis/Mass Spectrometry

The model peptides investigated in this section were *p*-trifluorotolylglycine methyl ester (3FpTolGOMe), *m*-trifluorotolylglycine methyl ester (3FmTolGOMe), *p*-tolylglycine methyl ester (pTolGOMe), and *m*-tolylglycine methyl ester (mTolGOMe). The *p*-trifluorotoluic acid, *m*-trifluorotoluic acid, *p*-toluic acid, and *m*-toluic acid were coupled to glycine methyl ester using the resin-bound carbodiimide as described in section 2.1.1. Synthesis and composition was confirmed as described in section 2.1.2.

Double resonance (DR) experiments were conducted to probe the potential serial dissociation pathways and were performed on a modified Bruker Esquire ITMS. The DR experiment was conducted by the excitation of the parent ion (M+H) while simultaneously ejecting one of the product ions, in our case the b^+ ion.

2.2.2 Kinetics

The kinetics experiment was conducted varying the ion trap activation time from 1ms up to 2000ms over four different CID energies (12, 14, 16, and 18) to monitor fragmentation as a function of time in the ion trap. Once the data was obtained the reaction curves were extrapolated by relative ion abundance as a function of activation time for each one of the CID energies mentioned. Pseudo reaction rate constants were extracted from the time-resolved CID profiles using the curve fit function within the Berkley-Madonna software.

The rate constants were then used to calculate pseudo energies of activation for each molecule. This was done by plotting the natural log of k versus one over the CID energy, the

slope of the line is then approximately equal to (-Ea/R). Solving for Ea we used the R value of 1.985877 $cal*K^{-1}*mol^{-1}$ to produce pseudo activation energies.

2.2.3 Molecular modeling

Density functional theory calculations were performed, using Gaussian 03, to determine the lowest-energy conformations of all relevant precursor, intermediate and post-reaction species, along with important transition states [21]. Final optimization and frequency calculations were conducted at the b3lyp/6-31+G(d,p) level of theory. Single point calculations were conducted at the b3lyp/6-311++G(3d,2p) to confirm energy trends.

CHAPTER 3

RESULTS

3.1 McLafferty

Model systems with nicotinic acid or betaine at the N-terminal sequence position were chosen for this study to test the use of the residues to fix the charge site. As noted earlier, there is both theoretical [22] and experimental, including IRMPD [23], evidence to support a mix of protonation sites for gas-phase peptide ions. The initial hypothesis for the NicGO*t*Bu system was that protonation would occur on the pyridine ring, thus preventing the added proton from effecting a change in conformation by migrating to and interacting with multiple amide carbonyl O atoms. The betaine residue instead contains a fixed positive charge because of the quaternary nitrogen.

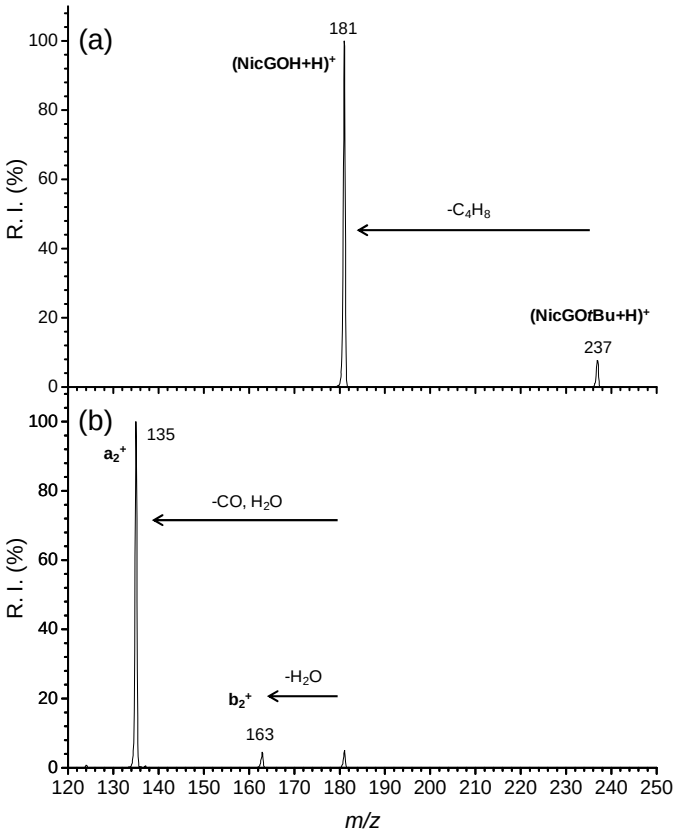

Figure 3.1-Tandem mass spectra starting from the protonated nicotinyl-glycine-*tert*-butyl ester $(NicGOtBu+H)^+$ using the quadrupole ion trap mass spectrometer: (a) dissociation of $(NicGOtBu+H)^+$; (b) dissociation (MS^3 stage) of $(NicGOH+H)^+$, product resulting from McLafferty rearrangement.

Tandem mass spectra generated from $(NicGOtBu+H)^+$ using the quadrupole ion trap mass spectrometer are shown in Figure 3.1. Similar results were observed for CID of $(BetGOtBu)^+$ (figure 3.2), and the observations for $(NicGOtBu+H)^+$ are discussed here because they are representative of both systems. Spectra for $(BetGOtBu)^+$ and

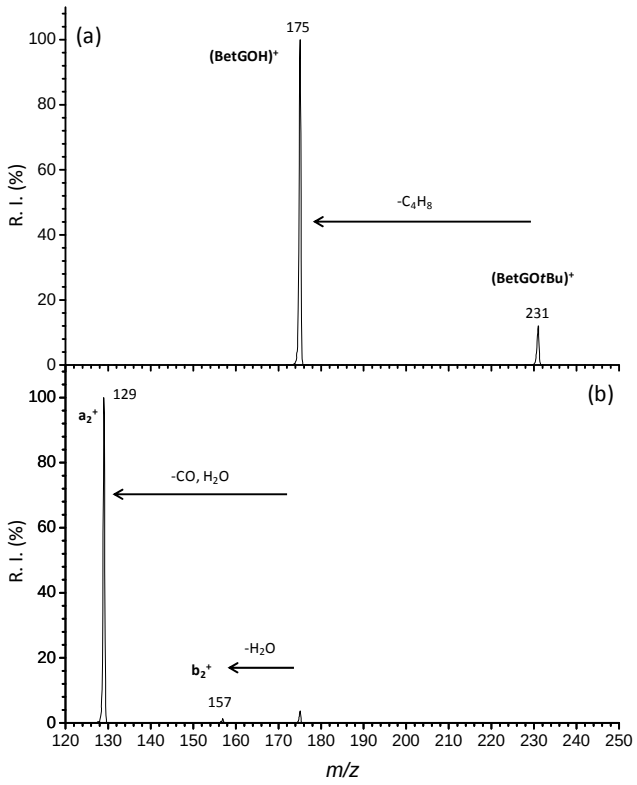

Figure 3.2-Tandem mass spectra starting from the betaine-glycine-*tert*-butyl ester $(BetGOtBu+H)^+$ using the quadrupole ion trap mass spectrometer: (a) dissociation of $(BetGO\textit{t}Bu+H)^+$; (b) dissociation (MS^3 stage) of $(BetGOH+H)^+$, product resulting from McLafferty rearrangement.

$(BetGOH)^+$ are provided in Figure 3.2. The only dissociation pathway observed following isolation and CID of $(NicGO\textit{t}Bu+H)^+$ at m/z 237 (MS/MS stage, Figure 3.1a) was elimination of 56 mass units (u), which is attributed to loss of isobutene from the *tert*-butyl ester group through McLafferty rearrangement (initial fragmentation of Scheme 3.1). The rearrangement furnishes the free-acid form of protonated nicotinyl-glycine, $(NicGOH+H)^+$, at m/z 181. Two pathways were observed following subsequent CID (MS^3 stage, figure 3.1b) of $(NicGOH+H)^+$: a minor pathway that involved formation of an ion at m/z 163 through elimination of 18 u (H_2O), and a major pathway for which the neutral loss was 46 u (H_2O + CO) to furnish an ion at m/z 135.

Using the conventional nomenclature for identification of peptide CID product ions [24-25], losses of 18 and 46 u correspond to formation of the b_2^+ and a_2^+ species, respectively, as shown in Scheme 3.1 for $(NicGO\textit{t}Bu+H)^+$. Within the context of the "oxazolone" pathway proposed to explain the general dissociation of protonated peptides [26-28], b_2^+ is an oxazolinone generated by nucleophilic attack upon the C-terminal carbonyl C atom, with associated *intra*-molecular transfer of an amide-position H atom. The

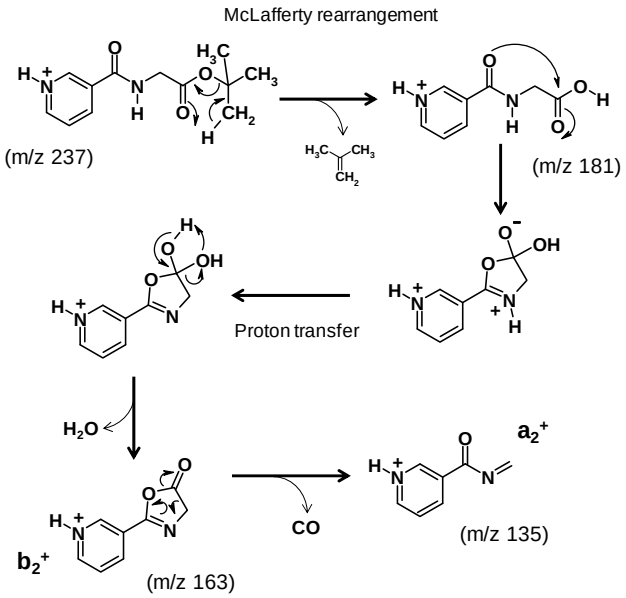

Scheme 3.1-Dissociation pathway for $(NicGOtBu+H)^+$ showing McLafferty rearrangement and formation of b_2^+ and a_2^+ via the "oxazolone" pathway.

oxazolinone then opens via the elimination of CO to produce a_2^+. Mechanistic studies strongly suggest that the b_n^+ species are cyclic products rather than linear acylium-type ions [26,27]. CID (MS^3 stage, spectrum not shown) of the m/z 163 product ion generated exclusively the a_2^+ species at m/z 135, consistent with the step-wise formation of a_2^+ from NicGOH. An alternative pathway for elimination of H_2O is a retro-Ritter or retro-Koch type reaction, as initially proposed by O'Hair and coworkers [29], which involves elimination of an amide position O atom. Such a pathway is particularly prominent in the dissociation of metal (Li^+ and Na^+) cationized peptide esters [30,31], and was thus considered in the present study. To determine the most probable mechanism by which the elimination of H_2O occurs, CID of protonated $(NicGOMe+H)^+$ (m/z 195) was examined (results not shown). CID of this species generated b_2^+ at m/z 163, and a_2^+ at m/z 135 (product ion m/z ratios identical to those observed for NicGOH) via elimination of 32 and 60 u, respectively: these neutral losses are consistent with a pathway analogous to that shown in Scheme 3.1, in that it begins with elimination of CH_3OH from the C-terminus of $(NicGOMe+H)^+$, and is followed by elimination of CO. Thus comparison of the CID results for NicGOH and NicGOMe suggests that the elimination of H_2O from the former occurs at the C-terminus, and thus represents generation of b_2^+. The

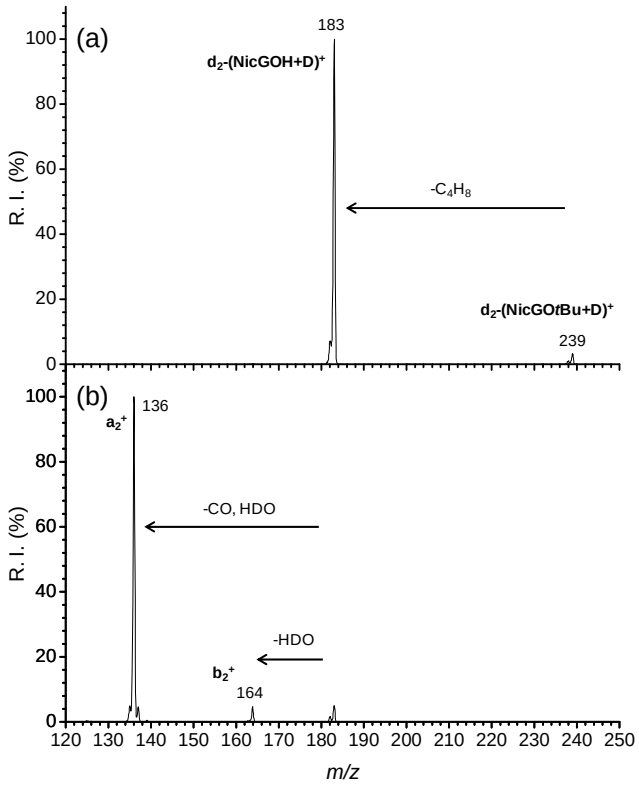

Figure 3.3- Tandem mass spectra starting from fully deuterium-exchanged nicotinyl-glycine-*tert*-butyl ester d2-(NicGOtBu+H)+ using the quadrupole ion trap mass spectrometer: (a) dissociation of d2-(NicGOtBu+H)+ , (b) dissociation (MS3 stage) of (NicGOH+H)+ product resulting from McLafferty rearrangement.

mass spectra shown in Figure 3.3 were generated from NicGO*t*Bu after incubation in a mixture of D_2O and CH_3OD to induce solution-phase H/D exchange (HDX). As shown in Figure 3.3a, CID (MS/MS stage) of d_2-(NicGOtBu+H)$^+$ (2 D atoms, at the ring N and amide N positions) at m/z 239 caused loss of 56 u, through McLafferty rearrangement and transfer of H, to furnish d_2-(NicGOH+H)$^+$ at m/z 183. Subsequent CID (figure 3.3b) of d_2-(NicGOH+H)$^+$ caused elimination of 19 u (HDO) to create b_2^+, and formation of a_2^+ at m/z 136 via the loss of 47 u (HDO and CO). Similar dissociation behavior was observed for d_1-(BetGO*t*Bu)$^+$ and d_1(BetGO*t*H)$^+$, for which CID spectra are in Figure 3.4.

The loss of HDO and CO following CID of the deuterium-exchanged forms of nicotinyl-glycine and betaine-glycine clearly demonstrates that an H atom is transferred from the departing butene neutral to the free-acid product ion following McLafferty-rearrangement, consistent with the earlier study of metal-cationized versions of acetylated peptide *tert*-butyl esters [32]. The free-acid forms of the peptides (i.e. the products resulting from McLafferty rearrangement) were isolated and stored in the ion trap mass spectrometer, without imposed collision activation, for periods ranging from 10 msec to 1

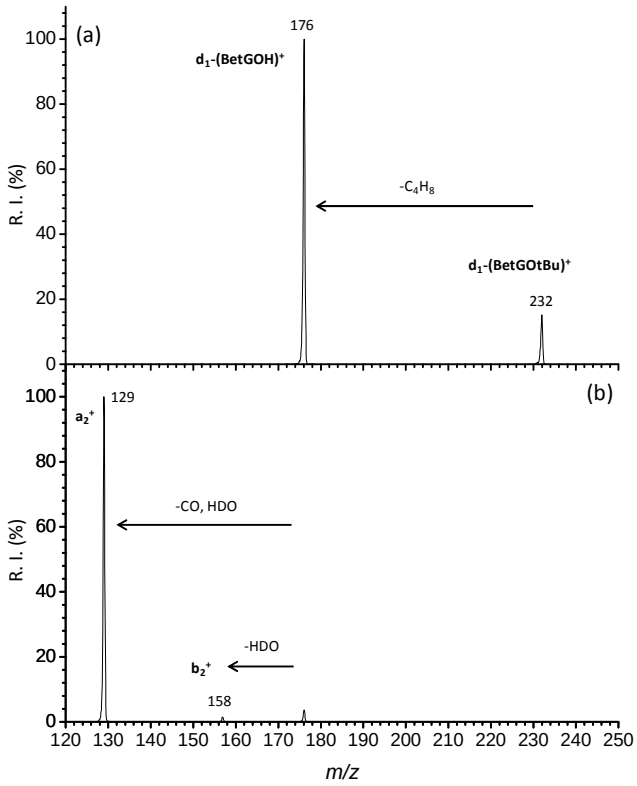

Figure 3.4- Tandem mass spectra starting from fully deuterium-exchanged betaine-glycine-*tert*-butyl ester d2-(BetGOtBu+H)+ using the quadrupole ion trap mass spectrometer: (a) dissociation of d2-(BetGOtBu+H)+ , (b) dissociation (MS3 stage) of (BetGOH+H)+ product resulting from McLafferty rearrangement.

sec. This experiment was performed to probe the tendency for D for H back exchange through collisions with ubiquitous H_2O in the ion trap. The test for back-exchange was conducted to ensure that the species generated after McLafferty rearrangement would not be susceptible to significant HDX that might occur through ion-molecule reactions with H_2O present in the ion transfer lenses in the FTICR instrument interfaced to the free-electron laser. In the quadrupole ion trap and at 1 x 10^{-6} torr of H_2O [33], no D for H back exchange was observed. This observation suggests that the tendency for exchange in the FTICR instrument is negligible, which is consistent with the IRMPD results discussed below.

Several potential conformations of protonated NicGOH, produced by DFT (B3LYP/6-311+g(d,p)), are shown in figure 3.5. The relative energies of each species (energy + zero point energy correction) are provided in Table 3.1. The lowest energy conformation predicted for $(NicGOH+H)^+$ by DFT, Nic_a, is one in which the peptide is protonated at the ring N atom of the nicotinic acid residue, and includes a hydrogen bonding interaction between the H atom of the amide group and the C-terminal carbonyl O atom.

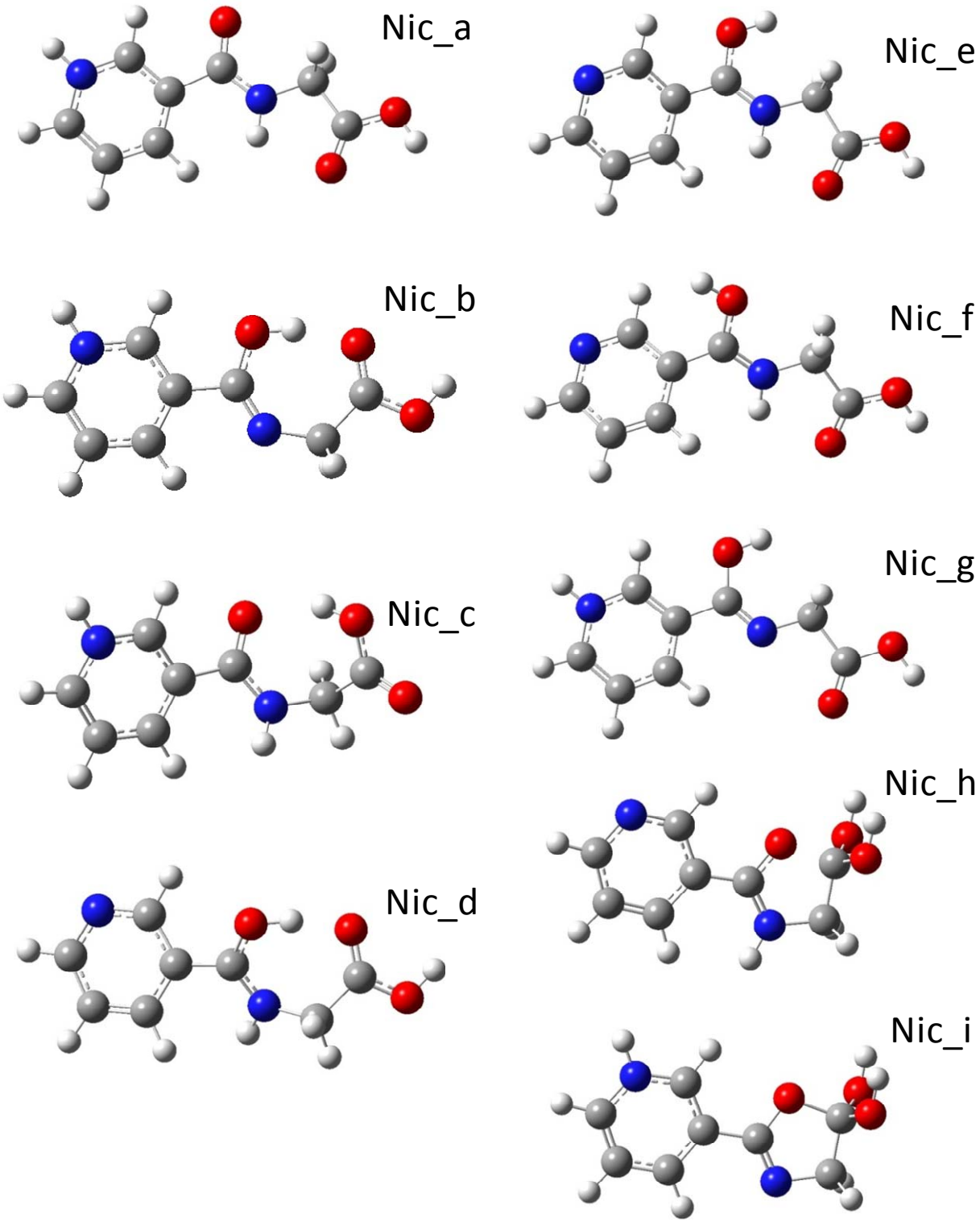

Figure 3.5- Potential conformations (Nic_a, Nic_b, Nic_c, Nic_d, Nic_d, Nic_e, Nic_f, Nic_g, Nic_h, and Nic_i) for $(NicGOH+H)^+$ as determined using DFT (B3LYP/6-311+g(d,p)).

Structure	Electronic energy (Hartrees)	Zero point correction (Hartrees)	ZPE corrected energy (Hartrees)	ΔE (kcal/mol)
Nic_a	-645.42760375	0.172342	-645.255262	0
Nic_b	-645.41396927	0.171945	-645.242025	+8.31
Nic_c	-645.41026594	0.172963	-645.237303	+11.27
Nic_d	-645.40820377	0.171706	-645.236497	+11.78
Nic_e	-645.40126874	0.171160	-645.230108	+15.78
Nic_f	-645.40673397	0.171548	-645.235186	+12.60
Nic_g	-645.40215344	0.171161	-645.230992	+15.23
Nic_h	-645.38800499	0.170890	-645.217115	+23.94
Nic_i	-645.38696168	0.171611	-645.215350	+25.05

Table 3.1 Relative Energies of $(NicGOH+H)^+$ conformational isomers.

Several structures that feature a proton "solvated" by interactions with the two carbonyl groups, Nic_b, Nic_c and Nic_d, were identified, and their relative energies are approximately 8-12 kcal/mol higher in energy than Nic_a. Other potential conformations that feature single amide O protonation, Nic_e, Nic_f and Nic_g, were all found to be at least 12 kcal/mol higher in energy. Two structures in which nucleophilic attack and cyclization has occurred were also identified (Nic_h and Nic_i); these species were > 20 kcal/mol higher than Nic_a.

Upon irradiation on resonance, both $(NicGOH+H)^+$ and $(BetGOH)^+$ eliminate H_2O and H_2O+CO, and these photofragment ions were used to generate the IRMPD spectra. Figure 3.6 compares the experimental IRMPD result for native (no deuterium exchange) $(NicGOH+H)^+$ to theoretical spectra for the four lowest energy conformations, Nic_a through Nic_d. Comparisons between the experimental spectrum and the theoretical spectra for structures Nic_e through Nic_h are provided in Figure 3.11. As noted earlier, the computed spectra are scaled by a factor 0.98 for direct comparison to the IRMPD

spectrum.

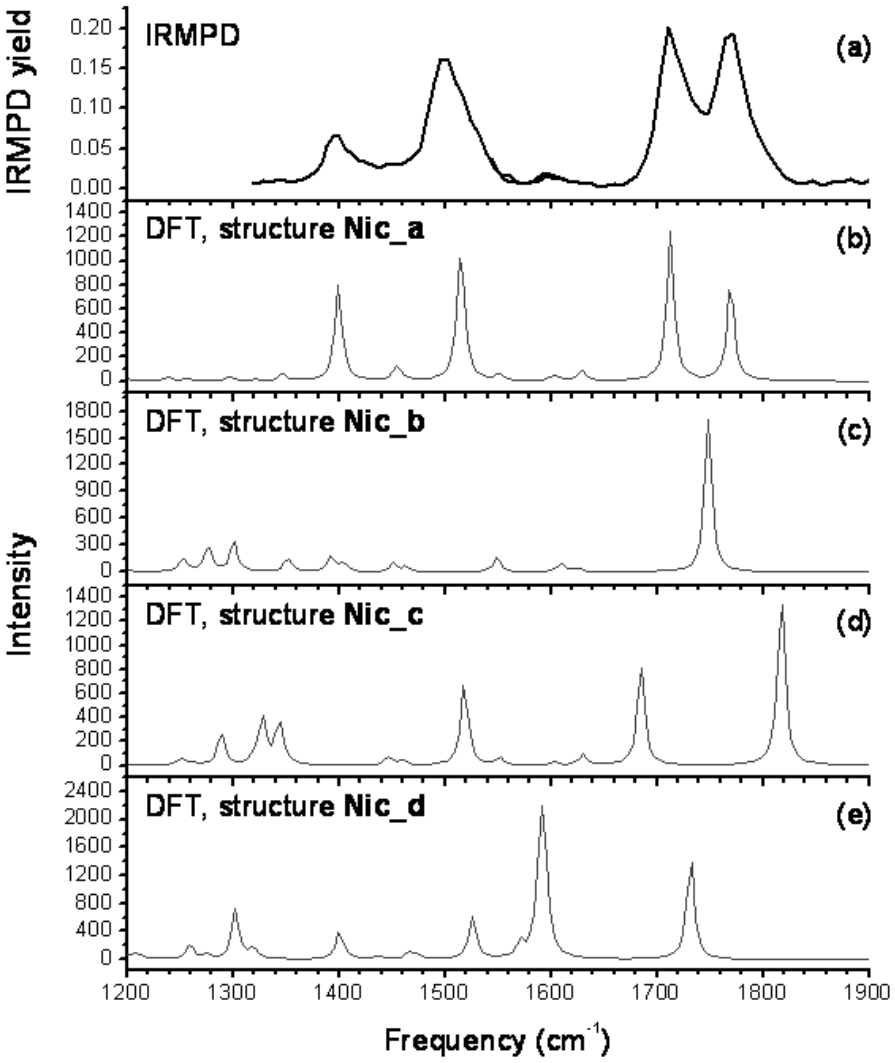

Figure 3.6- Comparison between IRMPD spectrum generated from $(NicGOH+H)^+$ (a) and theoretical spectra based on DFT calculations for structures: (b) Nic_a, (c) Nic_b, (d) Nic_c and (e) Nic_d. Conformations of Nic_a, Nic_b, Nic_c and Nic_d are provided in Figure 2.2.

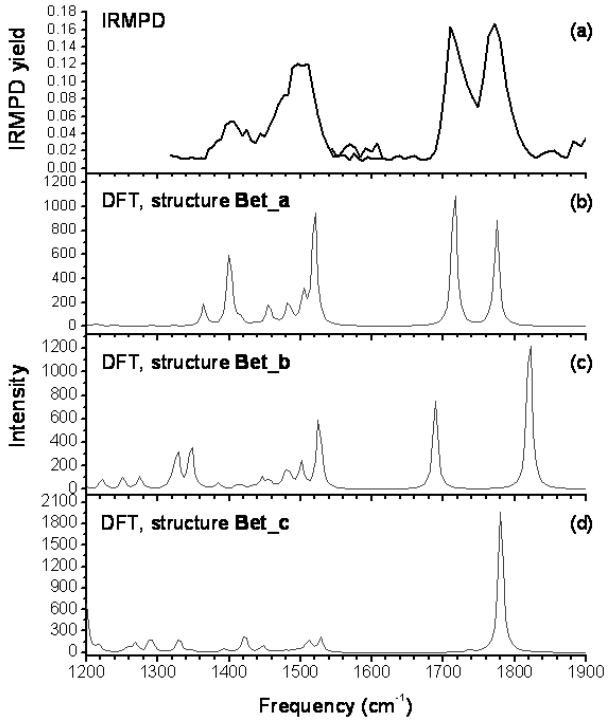

Figure 3.7- Comparison between IRMPD spectrum generated from BetGOH (a) and theoretical spectra based on DFT calculations for structures: (b) Bet_a and (c) Bet_b. Conformations of Bet_a and Bet_b are provided in Figure 2.4.

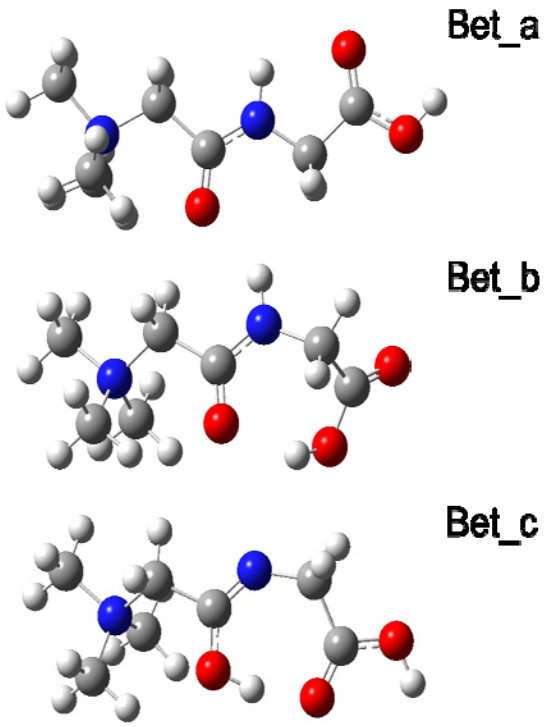

Figure 3.8- Potential conformations for $(BetGOH)^+$ as determined using DFT (B3LYP/6-311+g(d,p)).

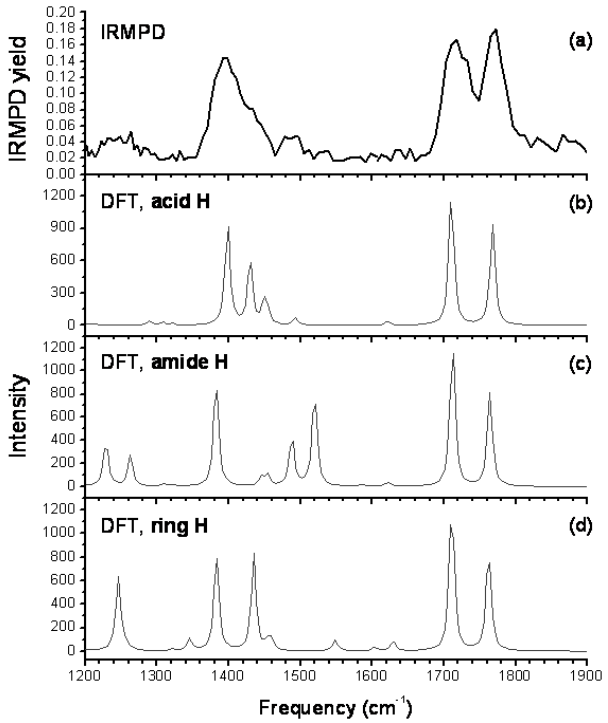

$(NicGOH+H)^+$ (a) and theoretical spectra based on DFT calculations for 3 different labeled isomers: (b) ring D, amide D and acid H; (c) ring D, amide H and acid D and (d) ring H, amide D and acid D. The conformation used to model the isomers was Nic_a, Figure 2.2.

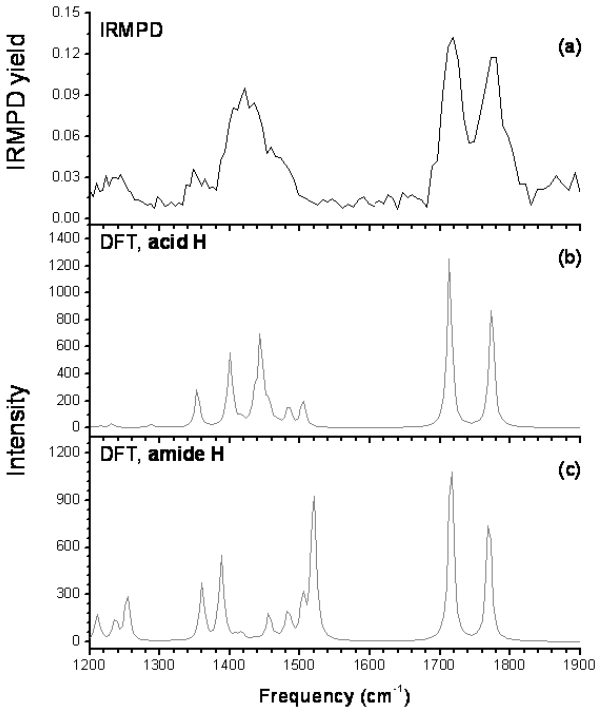

Figure 3.10- Comparison between IRMPD spectrum generated from d_1-$(BetGOH)^+$ (a) and theoretical spectra based on DFT calculations for 3 different labeled isomers: (b) amide D and acid H and (c) amide H and acid D. The conformation used to model the isomers was Bet_a, figure 2.4.

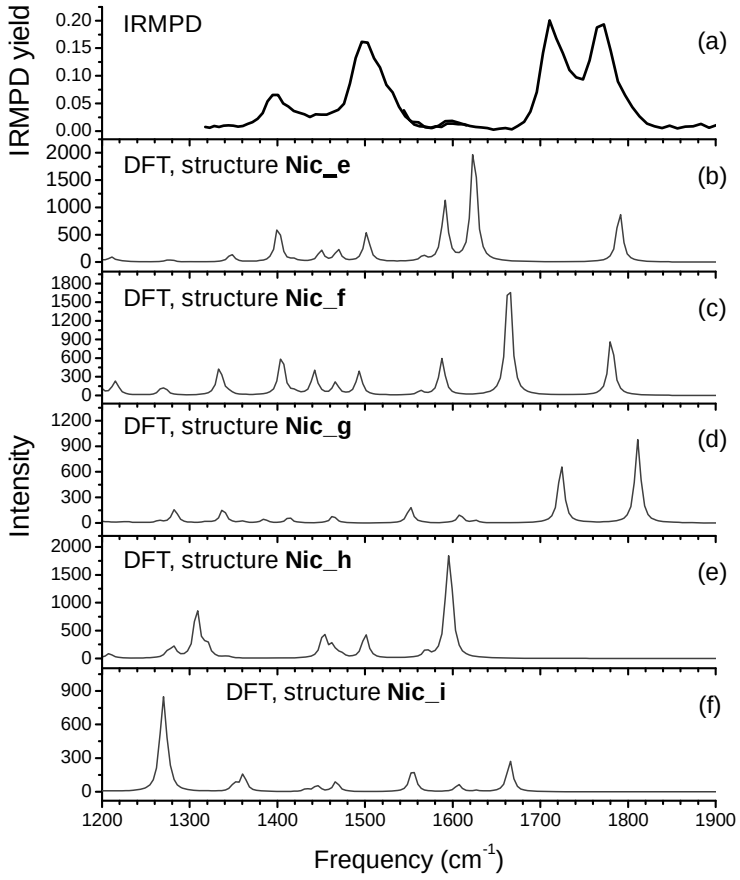

Figure 3.11- Comparison between IRMPD spectrum generated from $(NicGOH+H)^+$ (a) and theoretical spectra based on DFT calculations for structures: (b) Nic_e, (c) Nic_f, (d) Nic_g, (e) Nic_h, and (f) Nic_i. Conformations of Nic_a, Nic_b, Nic_c and Nic_d are provided in Figure 2.2.

Structure	E ectronic energy (Hartrees)	Zero point correction (Hartrees)	ZPE corrected energy (Hartrees)	ΔE (kcal/mol)
Bet_a	-610.92899952	0.233636	-610.695364	0
Bet_b	-610.91166897	0.234249	-610.677420	+11.260

Table 3.2 Relative energies of $(BetGOH)^+$ conformational isomers

As is apparent in Figures 3.6 and 3.11, the best match to the IRMPD spectrum, both in terms of the positions of the respective absorption frequencies and their relative intensities, is the lowest energy structure Nic_a in figure 3.11. Comparison to the DFT calculations allows assignment of the absorptions at calculated 1770 and 1710 cm^{-1} to the C=O stretches of the acid and amide groups, respectively. The absorption at calculated 1500 cm^{-1} corresponds to the amide II band, while the weaker absorption at calculated 1400 cm^{-1} is assigned to the C-C backbone stretch focused at the C-terminal G residue. Significant populations of the $(NicGOH+H)^+$ conformational isomers which feature solvation of a proton by amide carbonyl groups (Nic_b, Nic_c and Nic_d), can be ruled out based on the poorer agreement between the IRMPD and theoretical spectra in both the amide I and amide II regions. Potential conformations of gas-phase $(BetGOH)^+$ are

shown in Figure 3.8, and the relative energies of the species are provided in Table 3.2. The lowest energy conformation, Bet_a, is linear and features a hydrogen bonding interaction between the H atom of the amide group and the C- terminal carbonyl O atom. The structure in which the acid OH proton instead participates in a hydrogen bonding interaction with the amide carbonyl O atom, Bet_b, is several kcal/mol higher in energy. Figure 3.7 compares the experimental IRMPD spectrum of native (no deuterium exchange) $(BetGOH)^+$ to those predicted for species Bet_a and Bet_b. As is apparent in Figure 3.7, the best agreement between theory and experiment for the non-exchanged $(BetGOH)^+$ is for the species Bet_a. As in the case of $(NicGOH+H)^+$, comparison of the IRMPD spectrum generated from $(BetGOH)^+$ to the DFT calculations allows assignment of the absorptions at calculated 1770 and 1710 cm^{-1} to the C=O stretches of the acid and amide groups, respectively. The absorption at calculated 1500 cm^{-1} corresponds to the amide II band, while the weaker absorption at calculated 1400 cm^{-1} is assigned to the C-C backbone stretch focused at the C-terminal G residue. The amide II region is more congested for $(BetGOH)^+$ because of the addition of absorptions attributable to the tri-methyl amino group.

Figure 3.9a shows the the IRMPD spectrum derived from d_2-$(NicGOH+H)^+$ that was generated by McLafferty rearrangement of the deuterium-exchanged form of $(NicGO\textit{t}Bu+H)^+$. As demonstrated by the ion-trap CID results, McLafferty rearrangement causes transfer of an H atom to the peptide, presumably to the C-terminal acid group (the amide and pyridine ring N atoms carry D atoms as a result of solution-phase H/D exchange). The theoretical spectra shown in figure 3.9b-d are those predicted for d_2-$(NicGOH+H)^+$ with different arrangements of the two D and one H atom in exchangeable positions: 2.5b shows

the calculations for ring D, amide D and acid H; figure 3.9c shows the results for ring D, amide H and acid D and figure 3.9d shows the results for ring H, amide D and acid D. Adoption of isotope configurations modeled for figures 3.9c and 3.9d represent cases in which the H label generated by McLafferty rearrangement "scrambles" with the D atoms at the other exchangeable sites.

Comparison of spectra in Figure 3.9 suggests that the best match between theory and experiment is for the structure that features the H atom at the C-terminal acid group and with D at the ring N and amide N positions. As indicated in Figure 3.9b, DFT predicts that placement of a D atom at the amide N position of $(NicGOH+H)^+$ shifts the characteristic amide II band by calculated 70 cm^{-1} to approximately1430 cm^{-1}, which places the absorption in the high-frequency shoulder of the IRMPD peak in the region of 1360-1460 cm^{-1}. The major component in this same region is attributed to C-C stretches of the peptide backbone. It is also apparent from Figure 3.9, placement of D at the amide position has little influence on the position or intensity of the absorptions in the amide I region.

The presence of a significant population of gas-phase ions for which the D atom labeled has migrated to the amide N position would presumably be identified by an intense absorption in the vicinity of 1520 cm^{-1}, as predicted in the spectrum shown for the labeled peptide in Figure 3.9c and as observed in figures 3.6a and 3.6b for the non-labeled version of $(NicGOH+H)^+$. Migration of the H atom to the pyridyl ring, and a D atom to the C-terminal acid group, would presumably generate 2 absorptions of nearly equal intensity in the region of 1360-1460 cm^{-1}, and separated by a calculated 60 cm^{-1}. While the two predicted absorptions fall within the range of the peak between 1360 cm^{-1} and 1460 cm^{-1} in the

IRMPD spectrum, one would expect that contribution from the isotopic isomer modeled in Figure 3.9d would lead to a broader feature in this region, as well as a third strong absorption near 1240 cm^{-1}.

Figure 3.10 shows the comparison between the IRMPD spectrum derived from the d_1-$(BetGOH)^+$ ion generated by McLafferty rearrangement from the deuterium-exchanged form of the peptide. For the cationic $(BetGOH)^+$ peptide there are only two exchangeable sites, the amide N and acid OH groups. The spectra shown in Figure 3.10b and c are those predicted for d_1-$(BetGOH)^+$ with different arrangements of the D and H atoms: 3.10b shows the calculations for amide D and acid H; 3.10c shows the results for amide H and acid D. As for the d_2-$(NicGOH+H)^+$ cation, the best agreement between the theoretical spectra and the IRMPD spectrum for the deuterium exchanged form of $(BetGOH)^+$ is for the species with the H atom located on the free acid moiety.

3.2 Substituent Effects

Once CID was induced on the model peptides *m*TolGOMe, 3F*m*TolGOMe, *p*TolGOMe, and 3F*p*TolGOMe two distinct pathways were observed from the different electron withdrawing (trifluoromethyl) and electron donating (methyl) substituents. The electron withdrawing trifluoromethyl ($-CF_3$) substituent produced b^+ fragment ions for both *para*- and *meta*-positions (figure 3.12). The electron donating methyl ($-CH_3$) substituent produced both the b^+ ion as well as the acylium ion for both para- and meta-positions (figure 3.13). The dissociation patterns were further investigated with tandem MS/MS, MS^1 to MS^3. The trifluoromethyl substituent produced the a^+ ion with MS^2, acylium ion was not observed until MS^3. While the methyl substituent continued to produce the acylium ion in MS^2 and MS^3, the

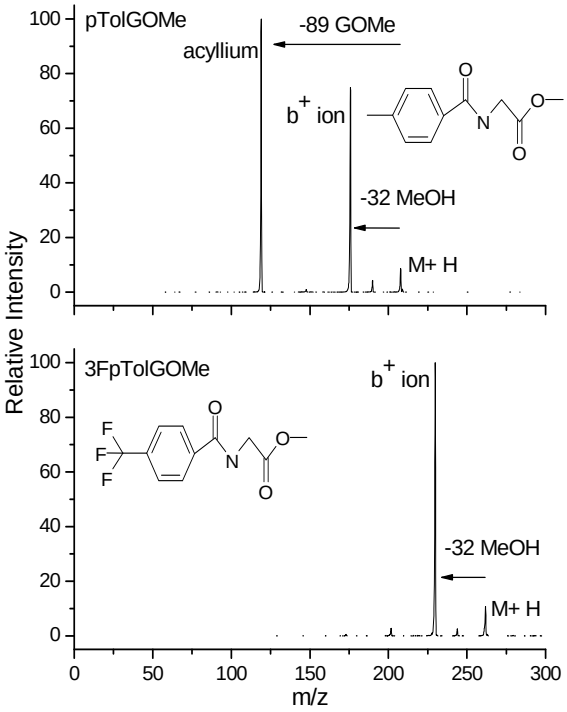

Figure 3.12-MS/MS comparison pTolGOMe to 3FpTolGOMe.

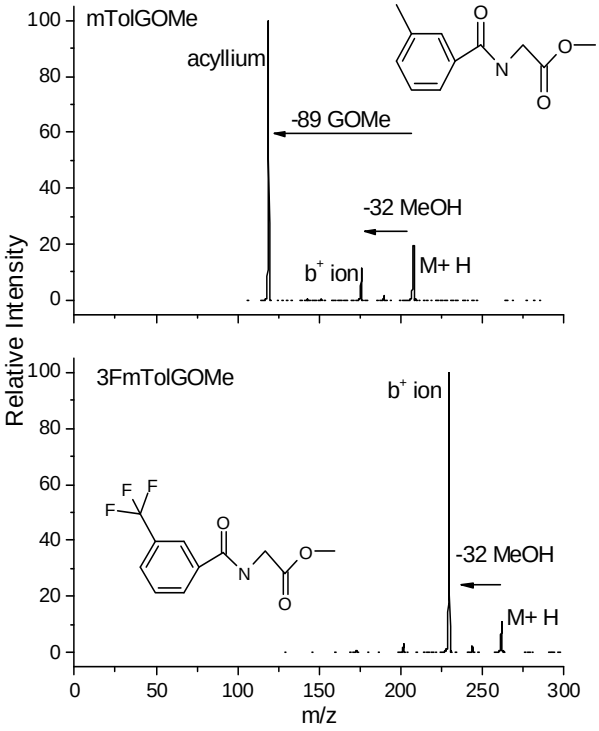

Figure 3.13-MS/MS comparison mTolGOMe to 3FmTolGOMe.

a^+ ion was observed in MS^2. The focus in this study was with MS/MS. Figures 3.12 and 3.13 show a comparison of the MS/MS fragmentation patterns for the *meta*- and *para*-position substituent, respectively.

The methyl substituent also exhibited differences in fragmentation between the *para*- and *meta*-positions. The *meta*-position fragmented with less energy and dissociated primarily to the acylium ion, with a ratio of 9:1 acylium to b^+ ion relative intensity. The *para*-position required more energy to fragment and had a dissociation ratio of 5:4 acylium to b^+ ion relative intensity.

The double resonance experiment demonstrated that both the b^+ and acylium ions are generated from the parent (M+H) ion, Figure 3.14. The double resonance spectrum in Figure

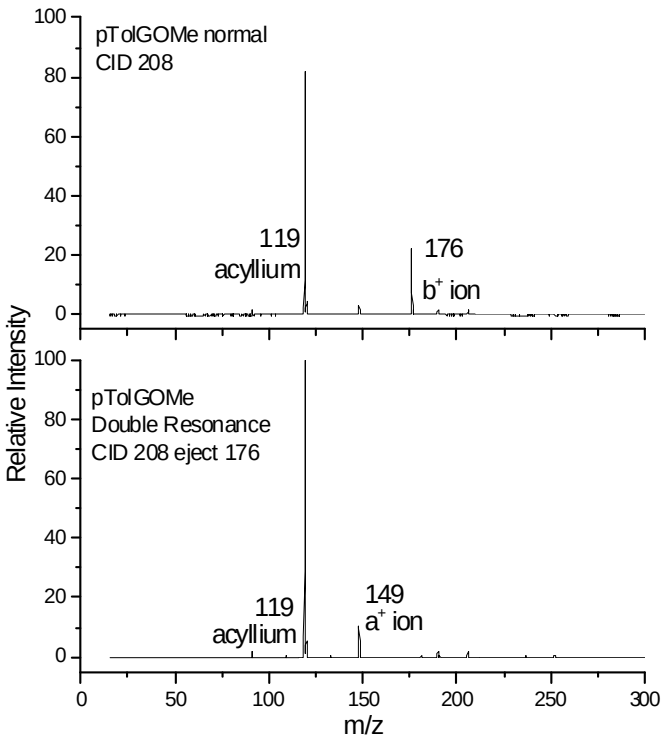

Figure 3.14-Double resonance experiment of pTolGOMe.

3.14 is representative of both the *p*TolGOMe and *m*TolGOMe experiments, in that simultaneous dissociation of the M+H and ejecting the b^+ ion result in both spectra exhibiting the acylium ion.

DFT calculations at the b3lyp/6-31+G(d,p) level of theory indicate that the formation of the b^+ is thermodynamically favored by 1.4 kcal/mol and 1.9 kcal/mol for the trifluoromethyl substituent in the meta- and para-positions respectively. The pathway to the formation of the b^+ ion is shown in scheme 3.2, a representative pathway followed for each *p*TolGOMe, *m*TolGOMe, 3F*m*TolGOMe, and 3F*p*TolGOMe. The molecule labeled xTol_1 or 3FxTol_1 was found to be the global minimum for the respective reactive configurations; therefore 0 kcal/mol for a given pathway. Table 3.3 has the relative energies with ZPE for each corresponding b^+ pathway. In each case TS_2 is the rate determining step or pseudo energy of activation.

Once the experimental data was imported into the Berkley-Madonna program the data was evaluated utilizing the curve fit function to obtain the rate constant. The experimental curve was visually fit to the Berkley-Madonna generated curve which generated the rate constant. The rate constant (k_1) evaluated was for the formation of the b^+ ion. The rate

constant value was evaluated for possible error by analyzing the lower and upper curve fit limits. The errors were all under six percent for k_1. This was done by refitting the experimental data low and high while maintaining an overall curve fit. The calculation was done according to equations 3.1.

$$k_{possible\ error} = (k_{high} - k_{low}) / k_{original} \quad (3.1)$$

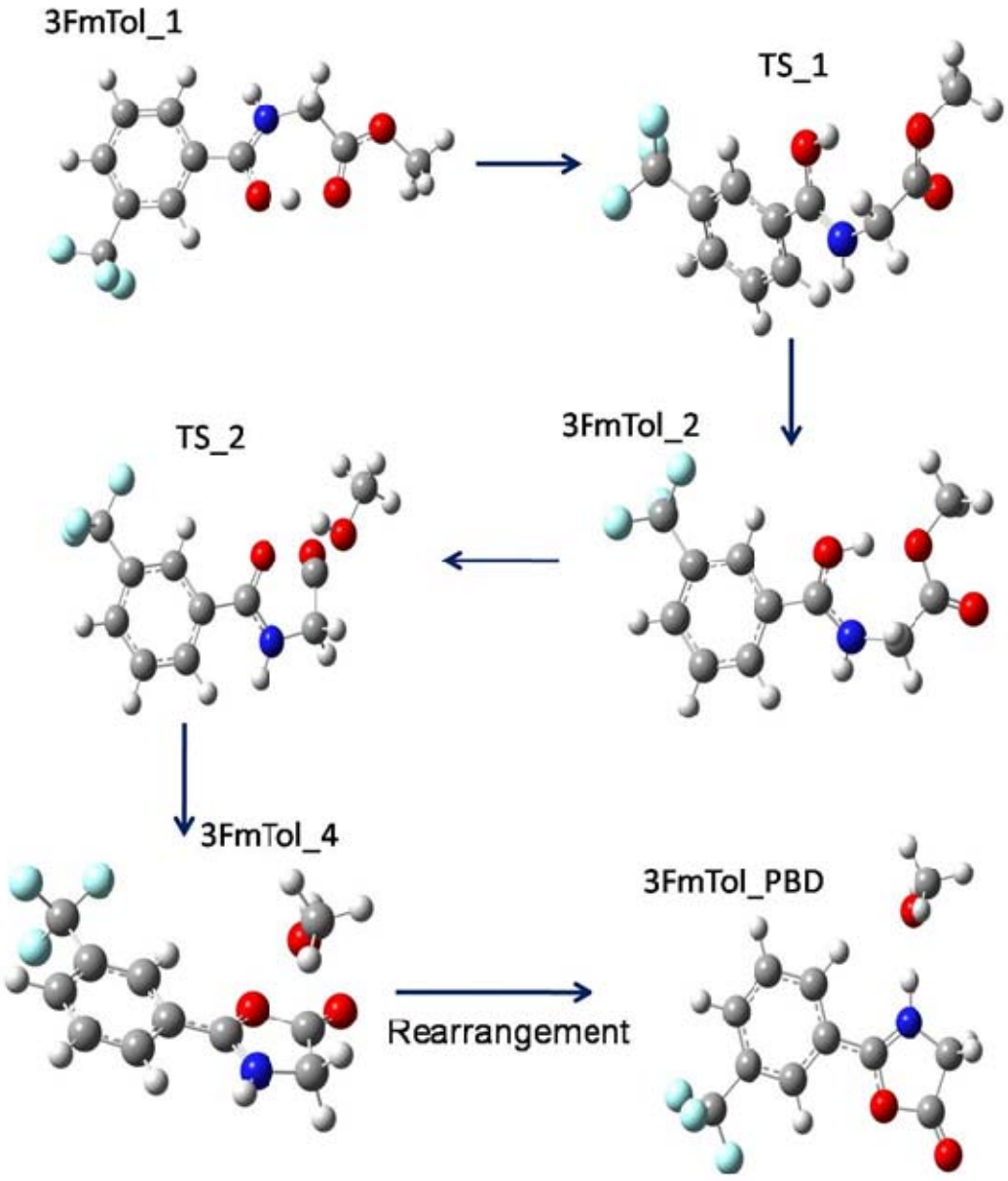

Scheme 3.2-Pathway for formation of b^+ ion (3F*m*TolGOMe).

Molecule	Relative Energies w/ ZPE		Molecule	Relative Energies w/ ZPE	
	para	meta		para	meta
xTol_1	0	0	3FxTol_1	0	0
TS_1	10.31625439	10.52960941	TS_1	11.2324201	11.16213899
xTol_2	6.617086528	6.815380679	3FxTol_2	7.2728351	7.074542103
TS_2	34.82614369	34.04113536	TS_2	32.8764777	32.63363155
xTol_4	16.2361808	16.44514147	3FxTol_4	17.5313604	17.41464364
xTol_PBD	9.617836436	9.821149478	3FxTol_PBD	10.3087261	10.34825737

Table 3.3-b^+ ion Relative energies with ZPE.

The pseudo activation energies support the DFT study in that the trifluoromethyl substituent dissociates with lower relative energy compared to the methyl substituent. Furthermore, the substituent in the *meta*-position dissociates more readily than when in the *para*-position. Tables 3.4 and 3.5 show pseudo rate constants and pseudo activation energies for each molecule studied, respectively.

Plotting the DFT pseudo-Ea versus those extracted from the experimental measurements using Berkley Madonna shows a linear relationship between experimental and theoretical data (Figure 3.15). This trend was then confirmed by a separate experiment where relative b^+ ion abundance was evaluated as a function of CID energy at two different activation times, 30 and 300 ms. Figure 3.16 illustrates this with the relative abundance as a function of volts, the lower the applied volt the faster the b^+ ion forms. Another correlation between figures 3.15 and 3.16 is that 3FmTol and 3FpTol are separated by very little energy for the formation of b^+ ion.

	3FmTolGOMe	3FpTolGOMe	pTolGOMe	mTolGOMe
CID	k_1	k_1	k_1	k_1
12	0.750795	0.718052	0.222961	0.290237
14	6.28917	5.928	0.9212	1.27522
16	15.781	15.4458	5.15811	7.33222
18	39.1694	39.6113	12.5408	14.4912

Table 3.4-Berkley Madonna pseudo rate constants for the formation of the b^+ ion.

	Pseudo Ea (b ion)
3FmTolGOMe	278.60394
3FpTolGOMe	282.67549
mTolGOMe	290.44977
pTolGOMe	295.98747

Table 3.5-Berkley Madonna pseudo Ea for the formation of the b^+ ion.

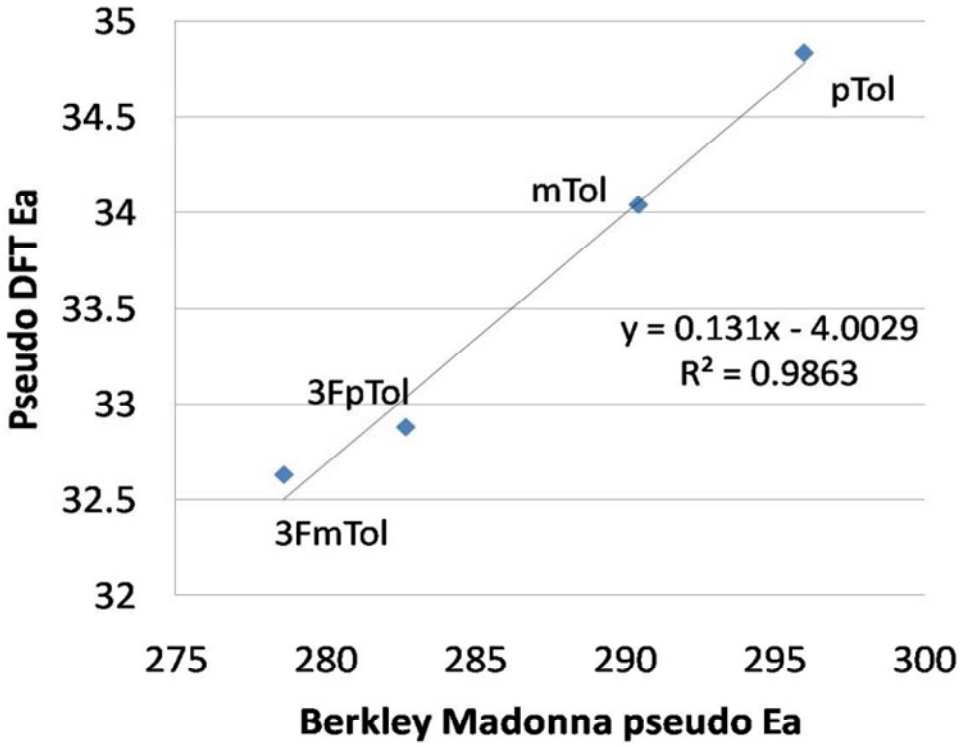

Figure 3.15-Pseudo DFT Ea vs. Berkley Madonna pseudo Ea.

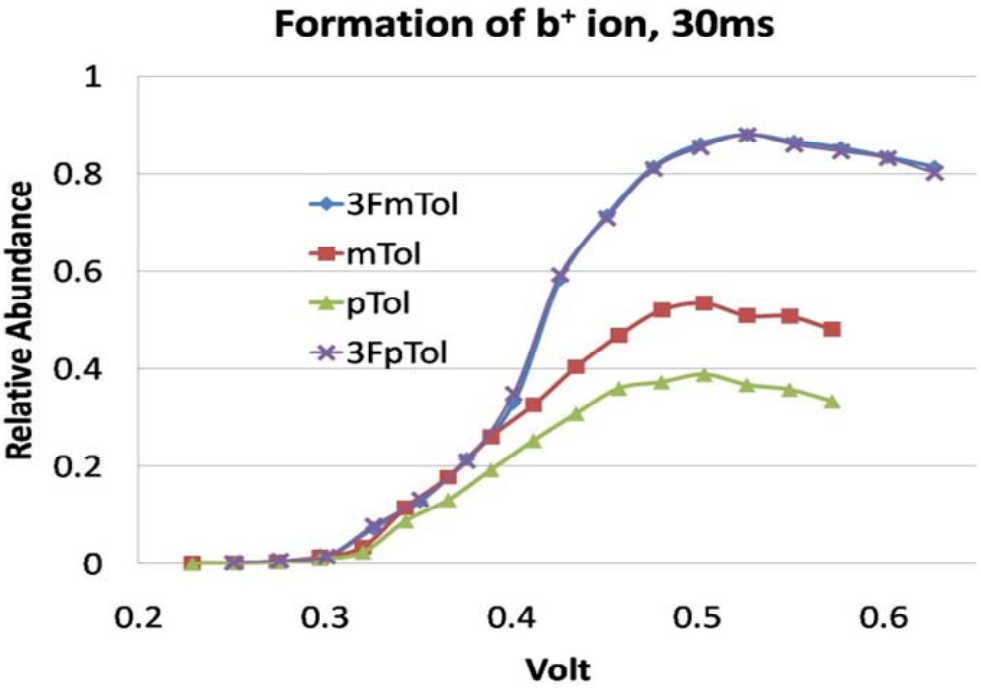

Figure 3.16-Relative b^+ ion abundance as a function of volts.

Chapter 4

Summary

4.1 **McLafferty**

The McLafferty rearrangement was confirmed utilizing MS and IRMPD instrumentation. The origin and mobility of the transferred hydrogen was determined by H/D exchange experiment with subsequent MS and IRMPD and comparing the IRMPD data to theoretical spectra generated by DFT calculations. It was determined that the *t*-butyl group transfers a hydrogen to the neighboring carbonyl group to form the carboxylic acid thereby losing the isobutene. The H atom does not transfer or scramble to another potential site. This experiment provides a benchmark for future experiments to probe or examine the mobility of the hydrogen.

4.2 **Substituent Effects**

There are definitive fragmentation differences between electron withdrawing and donating substituents. The primary fragmentation pathway for electron withdrawing substituent is the formation of the b^+ ion with the loss of neutral MeOH. In contrast electron donating substituents primarily produce the acylium ion with the loss of neutral GOMe. The position of the substituent also had an effect on the dissociation of the molecules for the methyl substituent. The results are further verified with a kinetics study by comparing theoretical and experimental data which has a linear relationship.

BIBLIOGRAPHY

Bibliography

[1] D. Hunt, J. Yates III, J. Shabanonowitz, S. Winston. C. Hauer. Proceedings of the National Academy of Sciences. 83, 6233-6237. 1986.

[2] K. Biemann. Biomedical and Environmental Mass Spectrometry. 16, 99-111. 1988.

[3] E. de Hoffmann and V. Stroobant. Mass Spectrometry Principles and Applications 3rd Ed. West Sussex, England : John Wiley & Sons Ltd., 2009.

[4] F. Rouessac and A. Rouessac. Chemical Analysis 2nd Ed. West Sussex, England : John Wiley & Sons Ltd, 2007, pp. 398-399.

[5] National High Magnetic Fiedl Laboratory [Online] 22 October 2009. http://www.magnet.fsu.edu/education/tutorials/tools/ionization_esi.html

[6] K. I. Ramachandran, G. Deepa, K. Namboori. Computational Chemistry and Molecular Modeling. Germany. Springer-Verlab Berlin Heidelberg, 2008.

[7] C. Cramer. Essentials of Computational Chemistry 2nd Ed. West Sussex, England : John Wiley & Sons Ltd., 2004.

[8] McLafferty, Fred W. *Analytical Chemistry*. 1956. 28, 306-316.

[9] H. Lioe, R. O'Hair. Org. Biomol. Chem. 3, 3618-3628. 2005.

[10] R. Vachet and S. McElvany. Journal of American Society for Mass Spectrometry. 10, 355-359. 1999.

[11] Paizs , Suhai. *Rapid Communications in Mass Spectrometry*. 2001. 15, 2307-2323.

[12] Roepstorff P, FohlmanJ. *Biomed. Mass Spectrometry*. 1984. 11, 601.

[13] Biemann K. *Biomed. Env. Mass Spectrometry*. 1988. 19, 99.

[14] N. C. Polfer, J. Oomens, D. T. Moore, G. von Helden, G. Meijer and R. C. Dunbar, *J. Am. Chem. Soc.*, 2006, 128, 905.

[15] A. G. Marshall, T.-C. L. Wang and T. L. Ricca, *J. Am. Chem. Soc.*, 1985, 107, 7893.

[16] V. N. Bagratashvili, V. S. Letokov, A. A. Makarov and E. A. Ryabov, *Multiple Photon Infrared Laser Photophysics and Photochemistry*, Harwood, Chur, Switzerland, 1985.

[17] J. Oomens, G. G. M. Tielens, B. G. Sartakov, G. von Helden and G. Meijer, *Astrophys. J.*, 2003, 591, 968.

[18] A. G. Marshall, C. L. Hendrickson and G. S. Jackson, *Mass Spectrom. Rev.*, 1998, 17, 1.

[19] C. T. Lee, W. T. Yang and R. G. Parr, *Phys. Rev. B.*, 1988, **37**, 785.

[20] A. D. Becke, *J. Chem. Phys.*, 1993, **98**, 5648.

[21] Gaussian 03, Revision D.01, M. J. Frisch, G. W. Trucks, H. B. Schlegel, G. E. Scuseria, M. A. Robb, J. R. Cheeseman, J. A. Montgomery, Jr., T. Vreven, K. N. Kudin, J. C. Burant, J. M. Millam, S. S. Iyengar, J. Tomasi, V. Barone, B. Mennucci, M. Cossi, G. Scalmani, N. Rega, G. A. Petersson, H. Nakatsuji, M. Hada, M. Ehara, K. Toyota, R. Fukuda, J. Hasegawa, M. Ishida, T. Nakajima, Y. Honda, O. Kitao, H. Nakai, M. Klene, X. Li, J. E. Knox, H. P. Hratchian, J. B. Cross, V. Bakken, C. Adamo, J. Jaramillo, R. Gomperts, R. E. Stratmann, O. Yazyev, A. J. Austin, R. Cammi, C. Pomelli, J. W. Ochterski, P. Y. Ayala, K. Morokuma, G. A. Voth, P. Salvador, J. J. Dannenberg, V. G. Zakrzewski, S. Dapprich, A. D. Daniels, M. C. Strain, O. Farkas, D. K. Malick, A. D. Rabuck, K. Raghavachari, J. B. Foresman, J. V. Ortiz, Q. Cui, A. G. Baboul, S. Clifford, J. Cioslowski, B. B. Stefanov, G. Liu, A. Liashenko, P. Piskorz, I. Komaromi, R. L. Martin, D. J. Fox, T. Keith, M. A. Al-Laham, C. Y. Peng, A. Nanayakkara, M. Challacombe, P. M. W. Gill, B. Johnson, W. Chen, M. W. Wong, C. Gonzalez, and J. A. Pople, Gaussian, Inc., Wallingford CT, 2004

[22] C. F. Rodriquez, A. Cunje, T. Shoeib, I. K. Chu, A. C. Hopkinson and K. W. M. Siu, *J. Am. Chem. Soc.*, 2001, **123**, 3006-3012.

[23] R. Wu and T. B. Mc Mahon, *J. Am. Chem. Soc.*, 2007, **129**, 11312-11313.

[24] P. Roepstorff and J. Fohlman, *Biomed. Env. Mass Spectrom.*, 1984, **11**, 601.

[25] K. Biemann, *Methods Enzymol.*, 1990, **193**, 455-465.

[26] T. Yalcin, C. Khouw, I. G. Csizmadia, M. R. Peterson and A. G. Harrison, *J. Am. Soc. Mass Spectrom*., 1995, **6,** 1165-1174.

[27] T. Yalcin, I. G. Csizmadia, M.B. Peterson and A. G. Harrison, *J. Am. Soc. Mass Spectrom*., 1996; **7**, 233-242

[28] B. Paizs and S. Suhai, *Mass Spectrom. Rev*., 2004, **24**, 508-548.

[29] G. E. Reid, R. J. Simpson and R. A. O'Hair, *J. Am. Soc. Mass Spectrom.* 1998, **9**, 945-956.

[30] V. Anbalagan, J. N. Patel, G. Niyakorn and M. J. Van Stipdonk, *Rapid Comm. Mass Spectrom.*, 2003, **17**, 291-300.

[31] E. R. Talaty, T. J. Cooper, D. L. Piland, D. J. Bateman, A. Syed, W. Stevenson and M. J. Van Stipdonk, *Rapid Comm. Mass Spectrom.*, 2006, **20**, 3007-3017.

[32] K. Bulleigh, A. Howard, T. Do, Q. Wu, V. Anbalagan and M. Van Stipdonk, *Rapid Comm. Mass Spectrom.*, 2006, **20**, 227-232.

[33] J. Lemaire, M. Boissel, G. Heninger, G. Mauclaire, G. Bellec, H. Mestdagh, A. Simon, S. Le Caer, J. M. Ortega, F. Glotin and P.Maitre, *Phys. Rev. Lett.*, 2002, **89**, 273002.